Effect of temperature-induced contact quality evolution on nanoscale friction

Wen Wang,[1,*] Xiang Zhou,[1] Linmao Qian,[1] and Q.-C. He[1,2]
[1]*School of Mechanical Engineering, Southwest Jiaotong University, 610031 Chengdu, China*
[2]*Université Gustave Eiffel, MSME, CNRS UMR 8208, F-77454 Marne-la-Vallée, France*

(Received 29 June 2022; revised 21 September 2022; accepted 26 September 2022; published 12 October 2022)

Multiple subcontacts formation/rupture and puckering the evolution of contact quality play crucial roles in modulating friction on two-dimensional lamellar materials but have up to now been studied separately in the field of nanotribology. In this work, by using variable temperature friction force microscopy in ultrahigh-vacuum conditions, we investigate friction on graphite surfaces with different numbers of free edges as a function of temperature from 295.0 to 100.0 K. We introduce subcontacts formation/rupture simply by changing temperature and tune the out-of-plane deformation compliance by changing the number of free edges. It is found that friction on a plane with large deformation compliance is constantly larger than that with small deformation compliance at cryogenic temperatures. While appearing to be influenced secondly by deformation compliance, the coefficients of friction increase, however, linearly with temperature. By performing systematic stick-slip measurements, the aforementioned separate friction mechanisms have been linked, where the temperature-induced increase of subcontacts rupture force can give rise to the frictional contact quality which additionally becomes more prominent on a plane with large deformation compliance at cryogenic temperatures. These results emphasize a way to vary the contact quality via temperature and demonstrate that the subcontacts formation/rupture and the contact quality must be correlatively accounted for.

DOI: 10.1103/PhysRevB.106.134103

I. INTRODUCTION

Friction, giving rise to an enormous amount of energy dissipation, is a key factor determining the efficiency and lifetime of moving components. In the field of tribology, materials with two-dimensional (2D) layered structures including graphite, transition metal dichalcogenides, and their derivative constructions, offer the possibility of substantially improving the reliability and prolonging the lifetime of their sliding components [1–5]. The unique mechanical and lubricative properties have stimulated expeditious advances in studying the fundamental factors influencing friction and wear like, e.g., the effects of sample thickness, crystalline orientation, sliding direction, and also the binding strength to substrate, etc. [6–15].

Specifically, due to the intrinsic weak interlayer van der Waals interaction and low out-of-plane bending rigidity of the 2D materials [16], the top layer may be lifted in front of the scanning tip, i.e., puckering effect [6,10,15]; as a result, friction tends to decrease with the increase of sample thickness [6,10,17]. Together with the lifting of the layer, the contact quality between the lifted layer and the scanning tip also evolves with scanning time, and the friction force gradually strengthens for a few initial atomic periods before reaching a constant value [13,15]. The contact quality and puckering effects become more pronounced as the deformation compliance of 2D materials increases and/or the binding between the 2D membranes and the substrate decreases [13,18,19]. The latter has been well documented from a fundamental perspective [10,15,20]. On the other hand, as the number of simultaneous subcontacts varies with temperature, the frictional contact quality may be tuned as well [21,22]. However, the coupling effects of subcontacts formation/rupture and deformation compliance on the evolving of contact quality as well as friction have yet to be addressed.

To study the aforementioned effects on friction, one of the most intriguing approaches is to analyze friction changes while simultaneously varying the deformation compliance and the subcontact formation/rupture. Contrary to the typical routine of preparing different samples, measuring friction on planes with different free edges at various temperatures directly allows us to modify the subcontacts and contact quality within the same sample. Consistent with the thermally activated multiple subcontacts formation/rupture process [21,23], the dry nanoscale friction on all planes exhibits a nonmonotonic behavior as a function of temperature with a friction peak at $T_{max} = 120.0 \pm 5.0$ K. Beyond that, friction force on a graphene layer with a larger out-of-plane deformation compliance is constantly higher than that on a graphene layer with a smaller deformation compliance when temperatures are below $T_t = 155.0 \pm 15.0$ K. In spite of the similar COFs (defined as the slope of friction vs normal force curve) on graphene layers with different deformation compliances, COFs additionally decrease linearly with the decrease of temperature. The atomic scale stick-slip measurements reveal that the anomalous friction behavior is essentially originated from the temperature-induced evolution of contact quality. Temperature can vary the number of simultaneous subcontacts as well as the contact rupture force, and as a result, the

*wangwen@swjtu.edu.cn

number of influenced atoms underneath the scanning tip and the interaction force between the substrate and the tip atoms are modified, i.e., the contact quality changes with temperature. Specifically, thanks to the increased contact rupture force when $T \leqslant T_t$, atoms underneath the scanning tip are likely to adjust their positions to form a more commensurate contact, and as a result, both friction and the puckered region in the front of the tip increase. This phenomenon becomes more pronounced on a plane with a larger deformation compliance.

II. METHODS

All frictional experiments were performed within an ultrahigh-vacuum (UHV) variable temperature VT-AFM/STM system (Scienta Omicron, Germany) employing a beam deflection detection scheme [24]. An average pressure of about 4×10^{-10} mbar was constantly maintained inside the UHV chamber during the whole sets of measurements. As a sample, we chose a commercial available squared highly oriented pyrolytic graphite (HOPG) (SPI-1) with the side length of ∼5 mm and thickness of approximately 2 mm. In order to control the sample temperature, the HOPG sample was firstly adhered onto a flat stainless-steel substrate by using a conductive epoxy glue (obtained from Epoxy Technology, USA). Afterwards, the aforementioned stainless-steel substrate was mechanically fixed to a low-temperature sample holder equipped with liquid nitrogen as a coolant [Fig. 1(a)] providing access to the temperature range of 300–95 K by adjusting either the flow rate of liquid N_2 or the power of resistance heating unit incorporated into the temperature control stage..

In order to prepare a clean graphite surface for the subsequent friction force measurements, the (0001) surface of the HOPG sample was first freshly cleaved by using the Scotch tape based exfoliation method just before being introduced into the vacuum chamber. To further remove residual adsorption from the graphite surface, the HOPG sample was additionally heated up to 500.0 K for 2.5 h inside the UHV chamber. All frictional and topographic measurements were performed in contact mode operation with the normal forces specified in the main text. Zero applied normal load is defined as the force acting on the cantilever at its equilibrium deflection. A PPP-LFMR cantilever with the normal stiffness of 1.4 N/m obtained from nanosensors was employed for the large area friction measurements and a CONTR cantilever with a small normal stiffness of 0.3 N/m obtained from Nanoworld was used for the atomic resolution stick-slip measurements. All lateral force values in this paper have been calibrated with the aid of the methods suggested by Bilas *et al.* through taking advantage of the piezo scanner bending during a large scan which can connect the torsion stiffness to the bending stiffness [25,26].

For the measurements at different temperatures, we first cooled the sample to a fixed temperature and then waited for at least 2 h until a stable state with negligible thermal drifts was reached. Additionally, we typically waited for several minutes after bringing the tip into contact with the cold graphite surface. During this period, a thermal equilibrium state between the tip and sample was established. It is better to conduct all measurements at the same area to reduce the experimental

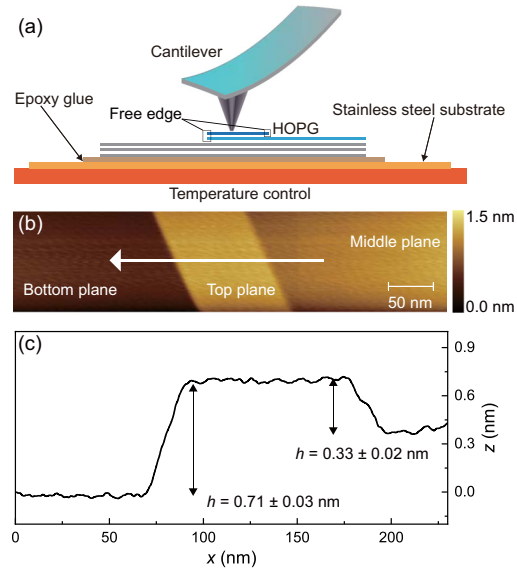

FIG. 1. Experimental setup and topography image of the graphite surfaces with different out-of-plane deformation compliance. (a) All experiments have been performed in UHV conditions using conventional friction force microscopy on a freshly cleaved HOPG sample, which was in contact with the variable temperature stage. (b) The topography image of the graphite surface obtained at $T = 295.0 \pm 0.1$ K with an externally applied normal load of 34.6 nN and a scan velocity of 250.0 nm/s. The bottom plane has no free edge within 2 μm scan range, the middle plane contains one free edge covered by the top plane, and the top plane comprises two free edges. (c) The representative cross-section profile across steps as indicated by the white arrow in (b) demonstrating the heights of the middle and top planes relative to the bottom plane are approximately 0.33 ± 0.02 nm and 0.71 ± 0.03 nm respectively.

uncertainties. To this end, we kept scanning on the graphite surface by using the contact mode and frequently compensating for the thermal drift. In our experiments, systematic frictional measurements were performed at the temperature varying from 100.0 to 295.0 K with the externally applied normal force varying from −4.9 to 34.6 nN. If not specified otherwise, the scanning velocity was fixed to $v = 250.0$ nm/s. To obtain sufficient statistics and reduce experimental errors, each force data point was extracted from the average values of total 100 frictional loops measured for each normal load while the error bars were calculated based on the standard error of the friction loops. During all measurements, both the topography image and the adhesion force signal showed no significant difference. After having finished all sets of measurements, we also heated the sample to room temperature $T = 297.7 \pm 0.1$ K to repeat the adhesion force measurement and found no obvious change of the adhesion indicating that the experiments were performed with negligible wear.

We deliberately found an area with one and two free edges induced during the mechanical cleavage process as illustrated in Fig. 1(a) in order to investigate the deformation compliance effects on friction. More specifically, the bottom plane has no free edge within 2 μm scan range, the middle plane contains one free edge covered by the top plane, and the top plane comprises two free edges; correspondingly, the top plane has the

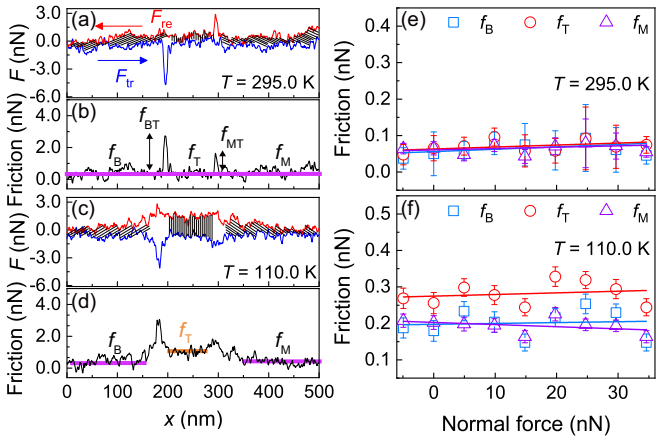

FIG. 2. The measured lateral and friction force on planes with different out-of-plane deformation compliance. (a) The measured lateral force curves at $T = 295.0 \pm 0.1$ K with the externally applied normal force $F_N = 19.8$ nN. (b) The calculated friction forces at $T = 295.0 \pm 0.1$ K. F_B, F_T, and F_M represent the calculated friction on the bottom, top, and middle planes, while F_{BT} and F_{MT} are the friction increase across the bilayer step and the monolayer step, respectively. (c) and (d) show the similar lateral force and friction force signal measured at $T = 110.0 \pm 0.1$ K exhibiting the similar behavior when scans cross the surface steps; however, friction on the top plane is larger than on the middle and bottom planes. (e) The measured friction forces at $T = 295.0 \pm 0.1$ K as a function of normal force from -4.9 to 34.6 nN where f_T, f_B, and f_M are almost the same. (f) The measured friction forces at $T = 110.0 \pm 0.1$ K, indicating that f_T is constantly larger than f_B and f_M. The error bars were calculated based on the standard error of the friction loops.

largest out-of-plane deformation compliance while the bottom plane has the smallest deformation compliance. Figure 1(b) shows the topographic image of such area (500 nm × 100 nm) obtained during scanning from right to left at $T = 295.0 \pm 0.1$ K with an externally applied normal load $F_N = 34.6$ nN. The cross-section profile shown in Fig. 1(b) was then plotted in Fig. 1(c), revealing that the heights of the middle and top planes relative to the bottom one are approximately 0.33 ± 0.02 and 0.71 ± 0.03 nm, respectively, i.e., mono- and bilayer graphene plane.

III. RESULTS AND DISCUSSION

We first present two representative lateral force curves obtained at $T = 295.0 \pm 0.1$ K and $T = 110.0 \pm 0.1$ K in Figs. 2(a) and 2(c) with the same normal force of 19.8 nN. The red lines (F_{re}) were obtained during scanning from right to left while the blue ones (F_{tr}) were recorded in the opposite scanning direction. Figures 2(b) and 2(d) then show the friction force calculated by $f = (F_{re} - F_{tr})/2$. For clarity, we divided the friction force curves into three parts according to the locations of free edges. Correspondingly, friction forces on the bottom, middle, and top planes are defined as f_B, f_M, and f_T, respectively; in the meantime, friction increases across the bilayer and monolayer edges are defined as f_{BT} and f_{MT}, as schematically illustrated in Fig. 2(b).

Despite the increase of friction [27,28] when the tip crosses step edges (see Supplemental Material [29] Figs. S1, S2, and S3 for more information about temperature and normal force effects on the friction increase), the most interesting thing is the observed friction difference on the above-mentioned planes induced by temperature, which has not been unveiled before. More specifically, as shown in Figs. 2(b) and 2(d), f_B, f_M, and f_T are almost the same at $T = 295.0 \pm 0.1$ K; however, f_T is notably larger than f_B and f_M at $T = 110.0 \pm 0.1$ K. Figures 2(e) and 2(f) then display the measured average f_T, f_B, and f_M at $T = 295.0 \pm 0.1$ and $T = 110.0 \pm 0.1$ K as a function of normal force varied from -4.9 to 34.6 nN. Only the friction forces on the flat planes slightly far from the free edges [shadow area in Figs. 2(a) and 2(c)] were used to calculate the average values of f_B, f_M, and f_T to exclude the edge effects. Within the normal force range, f_T is constantly larger than f_B and f_M at cryogenic temperature [Fig. 2(f)], demonstrating the remarkably reproducible results, while within the experimental uncertainties it is hard to distinguish f_B and f_M. This may be caused by the fact that the deformation compliance difference between the bottom and middle plane is relatively small since the middle plane is indeed fixed by the top graphene plane. The measurements carried out on a monolayer graphene with only one free edge confirm this conclusion (see Supplemental Material [29] Figs. S5 and S6 for more information, where a larger friction on a graphene plane with a free edge at cryogenic temperature was additionally observed). Within the normal force range, we find a linear relation between friction force and normal load at all temperatures checked in our measurements.

To vividly demonstrate the discoveries, we have plotted the f_T, f_B, and f_M measured with $F_N = 29.7$ nN as a function of temperature in Fig. 3(a) (see more information in Fig. S4 [29] about the temperature effects on friction). Consistent with the thermally activated multiple subcontacts formation and rupturing process [21–23], all friction curves show similar characteristic temperature dependencies. Initially friction forces increase with the decrease of temperature from ambient to low temperatures. Most prominently, a further reduction of temperature leads to a decrease of friction resulting in friction peaks at temperature $T_{max} = 120.0 \pm 5.0$ K. In addition, as T decreases below $T_t = 155.0 \pm 15.0$ K, f_T increases faster than f_B and f_M. As a comparison with the friction data, the simultaneously measured adhesion forces on three planes first decrease with the decrease of temperature before T_t and then abnormally increase indicating the change of contact between the atomic force microscopy (AFM) tip and the graphite surface [Fig. 3(b)]. Finally, adhesion forces decrease again with the further decrease of temperature.

The observed linear friction-normal load relationship allows us to extract temperature-dependent COFs by linearly fitting the friction vs normal force curves, which are less influenced by the change of tip radius and/or adhesion and make it possible to substantially compare the friction properties at different temperatures. The calculated temperature-dependent COFs are presented in Fig. 3(c). In spite of the different friction magnitudes, the COFs on all planes were found to be almost the same within the temperature range. In addition, COFs continuously decrease with the decrease of temperature.

Typically, for single asperity sliding friction, friction is monotonically increased with the decrease of temperature

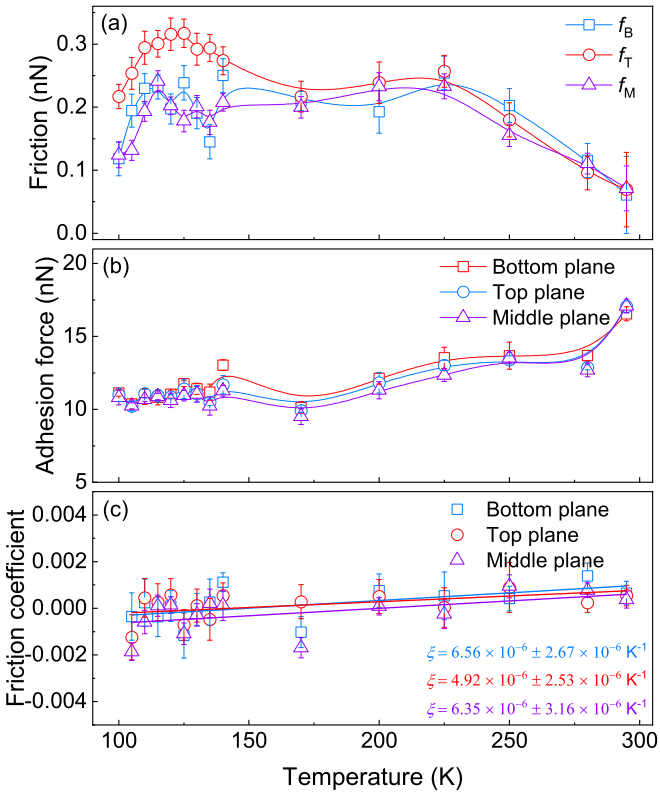

FIG. 3. The change of friction force, adhesion force, as well as the COFs on three planes as a function of temperature. (a) Temperature effects on the f_T, f_B, and f_M. Friction on all planes first increase and reach the maximum value around $T_{max} = 120.0 \pm 5.0$ K and then decrease with the further increase of temperature. In the meantime, f_T is larger than f_B and f_M when T is below $T_t = 155.0 \pm 15.0$ K. (b) The simultaneously measured adhesion forces on three planes as a function of temperature. Adhesion forces continuously decrease with the decrease of temperature while when the temperature decreases below T_t, an abnormal increase of adhesion force was observed. (c) Temperature effects on COFs on three planes. Within the experimental uncertainties, COFs on different planes show no obvious difference; alternately COFs decrease with the decrease of temperature. Scan parameters: $F_N = 29.7$ nN, scan size 500 nm × 100 nm.

[30,31]. Our results as shown in Figs. 2 and 3 unequivocally confirm the different frictional behavior on different planes at cryogenic temperatures which is strong evidence of a transition in the origin of friction. In comparison, prior friction force microscopy (FFM) investigations on an atomically flat graphite (0001) surface by using a silicon nitride tip under UHV conditions reported that both the friction forces and COFs increase exponentially with the decrease of temperature due to the thermally activated effects [32]. In addition, similar results were also observed on a flat MoS_2 surface from 500 to 220 K [33]. These two observations on flat surfaces are definitely opposite to the results observed here with free edges. Recently, friction experiments on graphene surfaces revealed an anomalous friction phenomenon related to the evolving of contact quality [6,7,10,11]. In general, friction change related to the contact quality is often considered as one of the main mechanisms in the energy dissipation process during sliding a nanosize tip on a surface of laminar materials [6,11]. In this picture, one could expect the graphene sheets to exhibit a transient behavior each time the AFM tip changes scanning direction.

To further scrutinize the temperature effects on the evolution of contact quality, we carried out atomic scale friction measurements on graphite surfaces as shown in Fig. 4(a). Specifically, the low plane has a small vertical deformation compliance while the high plane has a larger one. The inset curve shows the representative cross-section profile with the height difference of approximately 0.32 ± 0.02 nm. The left panels of Figs. 4(b) and 4(c) display the representative atomic stick-slip friction force maps recorded at $T = 295.0 \pm 0.1$ K on the high and low plane, respectively, while the left panels of Figs. 4(d) and 4(e) were obtained at $T = 109.0 \pm 0.1$ K (image size, 3 nm × 3 nm; normal load, 1.8 nN; scan velocity, 12 nm/s). Atomic-level stick slip on the graphite surface yields friction images with threefold symmetric patterns corresponding to the known symmetry of the lattices. In general, different crystallographic orientations of the honeycomb structure are associated to different stiffnesses, so depending on the crystallographic orientation friction caused by the puckering effect can vary a lot [7,12]. In fact, before carrying out the friction measurements, we manually chose planes which share the same orientation to within $0.6 \pm 0.2^\circ$ by carefully checking the stick-slip images. This means that the high and low planes are AB stacked and any friction differences related to the lattice orientation can be ruled out.

As shown by the representative friction loops in the right panels of Figs. 4(b)–4(e), the tip exhibits clear, periodic stick-slip motion, similar to that observed previously for graphene [10]. For room temperature measurements [Figs. 4(b) and 4(c)], only the regular atomic-scale stick slip has been observed. In contrast, for the cryogenic temperature measurements [Figs. 4(d) and 4(e)], the apparent lateral force strengthening (the lateral force at which each slip occurs slightly increases in magnitude during forward and backward scan, resulting in a tilted friction loop) can be observed and is strong evidence of the lifting of the graphene layer. The friction strengthening finally remains at a steady state after a few atomic periods on the low plane, while the lateral force measured on the high plane continuously increases and reaches a steady state around 4 nm due to the increased out-of-plane deformation compliance in the vicinity of the edge (see Supplemental Material Fig. S7 [29] for the large size stick-slip curves) [10,13,15].

Because of this friction strengthening, it is more meaningful to define the average friction force as the relative frictional energy dissipated per unit length. This amounts to first integrating the friction force over the forward and backward scans and then dividing the result by the total sliding distance. Figure 4(f) then displays the friction force on graphite planes as a function of the distance from the free edge as schematically illustrated by white rectangles in (a) at $T = 295.0 \pm 0.1$ K (lower panel) and $T = 109.0 \pm 0.1$ K (upper panel). Analogous to the result in Figs. 2 and 3, friction on the high plane with large deformation compliance is constantly larger than that on the low plane at cryogenic temperature. Additionally, when the scan area is slightly far from the edge, friction on the high plane decreases with the distance to the edge

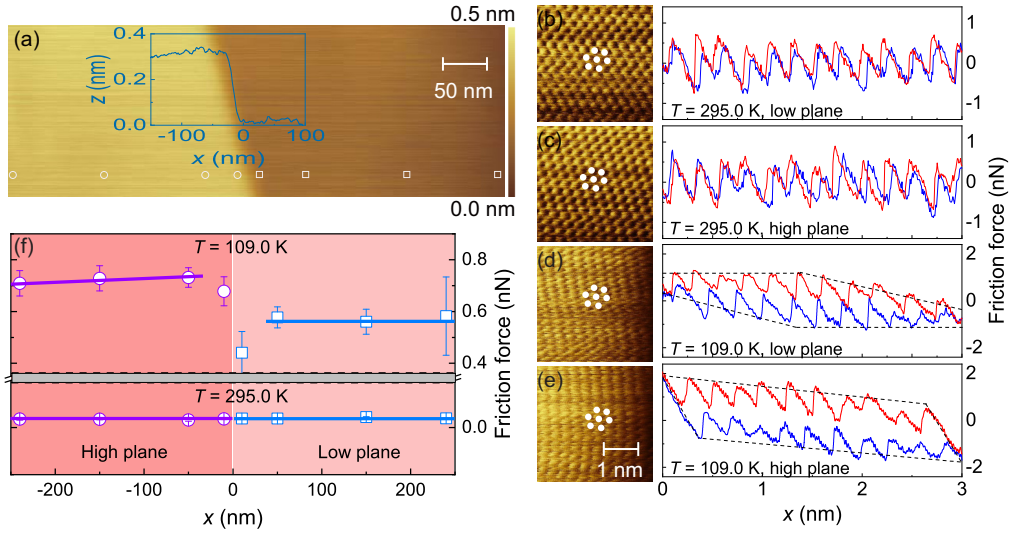

FIG. 4. Atomically resolved friction measurements on graphite surfaces. (a) The topography image of the graphite surface obtained at $T = 298.0 \pm 0.1$ K with an externally applied normal force of 0.0 nN and a scan velocity of 500 nm/s. The low plane contains no free edge while the high plane contains one free edge. The inset curve shows the representative cross-section profile showing the height difference is approximately 0.32 ± 0.02 nm. (b) and (c) show the representative atomic stick-slip friction force maps and curves recorded on the high and low planes of the graphite surface at $T = 295.0 \pm 0.1$ K while (d) and (e) show the similar results at $T = 109.0 \pm 0.1$ K. Image size, 3 nm × 3 nm; normal load, 1.8 nN; scan velocity, 12 nm/s. For room temperature measurements, only the regular atomic-scale stick-slip has been observed. In contrast, for the cryogenic temperature measurements, the apparent lateral force increase can be observed and this effect is more pronounced on the high plane. (f) Temperature dependence of friction force on graphite planes as a function of the distance from the edge as schematically illustrated by white symbols in (a). Friction on the high plane with a free edge is constantly larger than the low plane without free edges at cryogenic temperature. Friction is nearly independent of the distance to the edge at high temperature; however, friction on the high plane decreases with the distance while friction on the low plane stays almost independent of the distance at cryogenic temperature. When the scan area is very close to the edge, a drastic decrease of friction on both planes at cryogenic temperature was observed.

while friction on the low plane is nearly independent of the distance at cryogenic temperature, which agrees with the fact that the deformation compliance of the high plane decreases with the distance to the edge. Finally, a drastic decrease of friction on both planes at cryogenic temperature when the scan area is very close to the edge was observed. This may be caused by the excess interaction between the scanning tip and the free edge, although we do not have a good understanding at this point.

The friction strengthening is a manifestation of the contact quality evolution [10,15]. As the temperature decreases, the quality of contact between the tip and the graphene layer improves on one hand due to the temperature-induced subcontacts formation [23], and on the other hand due to the suppressed thermal fluctuation, and thus larger friction would be expected. As a result, the scan distance or time for the strengthening effect to stop influencing friction increases with the decrease of temperature [Figs. 4(b)–4(e)]. The slope of the lateral force in the strengthening region reflects the overall lateral stiffness of the AFM cantilever, tip, and the substrate. Nevertheless, it is difficult to conclude how the slope of lateral force changes with temperature due to the large experimental uncertainties. However, the slope on the high plane is smaller than that on the low plane, indicating that the deformability of the high plane with smaller dimensions is larger than that of the low plane.

The interlayer binding energy of graphene layers may change with temperature. Nevertheless, no quantitative data is available so far and there is a need for qualitatively understanding the observed friction phenomena. But according to the previous results, we estimate that within the temperature range checked here, the change of graphite interlayer binding energy would be relatively small (less than 2%) [16,34]. In addition, the simultaneously measured adhesion force between the silicon tip and the substrate did not change too much. Thus any mechanisms related to the binding energy change can be reasonably excluded.

The distinct velocity effect on friction force can be an important indicator to understand the physical mechanisms behind the temperature dependence of friction. Figure 5 shows the friction force measured on the same flat monolayer terrace (high plane) and the base plane (low plane) as a function of sliding velocity from 12.5 to 10 000 nm/s at temperatures of 300.0 ± 0.1 and 130.0 ± 0.1 K. For the high-temperature measurements, friction forces on the high and low planes exhibit an analogous behavior that is logarithmically dependent on the sliding velocity, which can be readily explained by the thermally activated process within the framework of a Prandtl-Tomlinson (PT) model [35]. However, friction both on the high and the low plane shows a distinct peak with the increase of sliding velocity. Moreover, the high plane with a larger deformability shows a narrower but higher peak. A similar friction peak was observed before [21,23] and explained within the framework of multiple subcontacts formation/rupture [21–23]. Beyond that, the friction difference between the high and low planes depends on the sliding velocity. Friction force on the high plane is always larger than that on the low plane for low sliding velocity. The situation

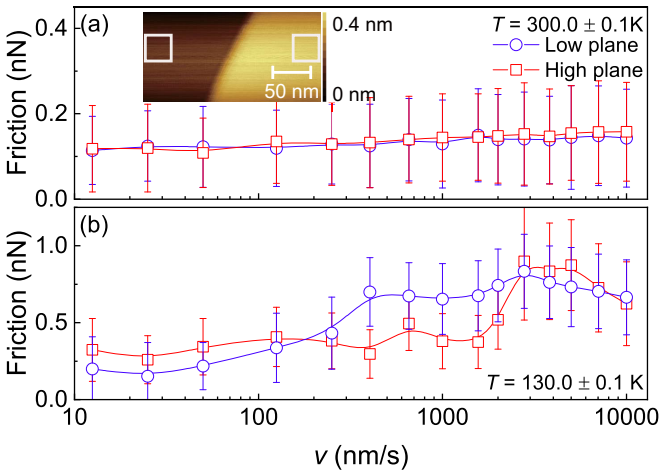

FIG. 5. Velocity effects on friction measured on different planes in the vicinity of the monolayer step edge. (a) Friction forces on the low and high planes obtained at $T = 300.0 \pm 0.1$ K. The inset image shows the topography information of the high monolayer terrace and base plane with the white rectangles indicating the friction measure regions. (b) The measured friction forces on the same planes at $T = 130.0 \pm 0.1$ K. At cryogenic temperatures, a distinct friction peak on both planes was observed due to the thermally activated multiple subcontacts formation and rupture. Friction measurement parameters: normal force $F_N = 22.5$ nN, scan size 50 nm × 50 nm.

becomes ambiguous for high velocity involving the dynamics of the puckered regions which need more theoretical works so as to understand the dynamic process.

Based on these arguments, we propose the following phenomenological physical picture based on the evolution of contact quality and thermally activate multiple subcontacts formation/rupture for the abnormal friction behavior. As temperature decreases, the number of simultaneous subcontacts decreases, while on the contrary the contact rupture force increases, so their competition leads to a friction peak at $T_{\max}$ [21–23]. In addition, due to the enhanced rupture force (or interaction force) at low temperature ($T \leqslant T_t$), atoms underneath the tip are strongly influenced and more likely rearrange their position to form a more commensurate or a better-pinned interface, thus the strengthening of friction is observed. At high temperature, the contact quality effect disappears due to the insufficient contact rupture forces and/or the enhanced thermal fluctuation. In addition, atoms belonging to a plane with a larger deformation compliance (less constrained) are able to adjust their position more easily because of the increased susceptibility to out-of-plane elastic deformation; therefore, more pronounced friction strength and greater friction is likely. Previous molecular dynamics results [15] also revealed that the out-of-plane deformation or pucker, mostly constrained to the topmost graphene layer, is a persistent feature and can occur even for bulk graphite samples. Therefore, a larger puckered region is correlated with a larger friction [15]. Under this circumstance, one can also imagine a temperature and deformation compliance dependence of the puckered region. However, we have no direct evidence since it is really difficult to characterize the deformed region in such a small scale. Finally, at cryogenic temperatures, the suppressed thermal fluctuation may also give rise to the contact quality effects.

IV. CONCLUSION

In this paper, we study fundamental frictional energy dissipation processes on graphite surfaces of both physical obsession and technological significance. We present experimental measurements of the temperature effects on the atomic friction on graphite surfaces with different out-of-plane deformation compliances in UHV conditions. The experimental results reveal a nonmonotonic variation of friction with temperature consistent with the thermally activated multiple subcontacts formation/rupture process. In addition, friction force on a plane of large compliance is constantly larger than that of small deformation compliance at cryogenic temperatures. In contrast, the measured COFs are independent of the deformation compliance, which decrease linearly with the decrease of temperature. The anomalous friction behavior is originated from the temperature-induced evolution of contact quality which becomes more prominent on one hand due to the increased contact rupture force and suppressed thermal fluctuation at cryogenic temperature, and on the other hand due to the increased high out-of-plane deformation compliance. This peculiar behavior has profound consequences for tribological properties of graphite/graphene based devices and may open the stimulating foreground of tuning friction of lamellar materials. In addition, the link of temperature-induced subcontacts formation/rupture effect is of great importance for building a more realistic model.

ACKNOWLEDGMENTS

The authors acknowledge the financial support by the NSFC (Grants No. 12172309, No. 11890672, No. 11890673, No. 61704013, and No. 11602205), NSFSC (Grant No. 2022NSFSC1917), and the Analytical and Testing Center of Southwest Jiaotong University for the FFM measurements. W.W. conceived the study. W.W. designed the experiment(s), W.W. and X.Z. conducted the experiment(s), W.W. and X.Z. analyzed the results. All authors discussed the results and contributed to writing the paper.

The authors declare no competing financial interests.

[1] H. Li, J. Wang, S. Gao, Q. Chen, L. Peng, K. Liu, and X. Wei, Adv. Mater. **29**, 1701474 (2017).

[2] D. Berman, S. A. Deshmukh, S. K. Sankaranarayanan, A. Erdemir, and A. V. Sumant, Science **348**, 1118 (2015).

[3] Z. Zhang, Y. Du, S. Huang, F. Meng, L. Chen, W. Xie, K. Chang, C. Zhang, Y. Lu, C.-T. Lin *et al.*, Adv. Sci. **7**, 1903239 (2020).

[4] S. Kawai, A. Benassi, E. Gnecco, H. Söde, R. Pawlak, X. Feng, K. Müllen, D. Passerone, C. A. Pignedoli, P. Ruffieux *et al.*, Science **351**, 957 (2016).

[5] D. Dietzel, M. Feldmann, U. D. Schwarz, H. Fuchs, and A. Schirmeisen, Phys. Rev. Lett. **111**, 235502 (2013).
[6] H. Lee, N. Lee, Y. Seo, J. Eom, and S. Lee, Nanotechnology **20**, 325701 (2009).
[7] M. V. Rastei, B. Heinrich, and J. L. Gallani, Phys. Rev. Lett. **111**, 084301 (2013).
[8] M. Dienwiebel, G. S. Verhoeven, N. Pradeep, J. W. M. Frenken, J. A. Heimberg, and H. W. Zandbergen, Phys. Rev. Lett. **92**, 126101 (2004).
[9] Z. Ye and A. Martini, Appl. Phys. Lett. **106**, 231603 (2015).
[10] C. Lee, Q. Li, W. Kalb, X.-Z. Liu, H. Berger, R. W. Carpick, and J. Hone, Science **328**, 76 (2010).
[11] Z. Deng, A. Smolyanitsky, Q. Li, X.-Q. Feng, and R. J. Cannara, Nat. Mater. **11**, 1032 (2012).
[12] M. V. Rastei, P. Guzmán, and J. L. Gallani, Phys. Rev. B **90**, 041409(R) (2014).
[13] S. Zhang, Y. Hou, S. Li, L. Liu, Z. Zhang, X.-Q. Feng, and Q. Li, Proc. Natl. Acad. Sci. USA **116**, 24452 (2019).
[14] Y. Dong, J. Phys. D **47**, 055305 (2014).
[15] S. Li, Q. Li, R. W. Carpick, P. Gumbsch, X. Z. Liu, X. Ding, J. Sun, and J. Li, Nature (London) **539**, 541 (2016).
[16] W. Wang, S. Dai, X. Li, J. Yang, D. J. Srolovitz, and Q. Zheng, Nat. Commun. **6**, 7853 (2015).
[17] Q. Li, C. Lee, R. W. Carpick, and J. Hone, Physica Status Solidi B **247**, 2909 (2010).
[18] X. Zeng, Y. Peng, and H. Lang, Carbon **118**, 233 (2017).
[19] B. Shi, X. Gan, H. Lang, K. Zou, L. Wang, J. Sun, Y. Lu, and Y. Peng, Nanoscale **13**, 16860 (2021).
[20] Y. Peng, X. Zeng, K. Yu, and H. Lang, Carbon **163**, 186 (2020).
[21] I. Barel, M. Urbakh, L. Jansen, and A. Schirmeisen, Phys. Rev. Lett. **104**, 066104 (2010).
[22] I. Barel, M. Urbakh, L. Jansen, and A. Schirmeisen, Tribol. Lett. **39**, 311 (2010).
[23] W. Ouyang, Y. Cheng, M. Ma, and M. Urbakh, J. Mech. Phys. Solids **137**, 103880 (2020).
[24] G. Meyer and N. M. Amer, Appl. Phys. Lett. **57**, 2089 (1990).
[25] P. Bilas, L. Romana, B. Kraus, Y. Bercion, and J. Mansot, Rev. Sci. Instrum. **75**, 415 (2004).
[26] W. Wang, D. Dietzel, and A. Schirmeisen, Sci. Adv. **6**, eaay0165 (2020).
[27] P. Steiner, E. Gnecco, F. Krok, J. Budzioch, L. Walczak, J. Konior, M. Szymonski, and E. Meyer, Phys. Rev. Lett. **106**, 186104 (2011).
[28] T. Müller, M. Lohrmann, T. Kässer, O. Marti, J. Mlynek, and G. Krausch, Phys. Rev. Lett. **79**, 5066 (1997).
[29] See Supplemental Material at http://link.aps.org/supplemental/10.1103/PhysRevB.106.134103 for details on the friction force across surface steps, additional results, and atomic stick-slip measurements.
[30] L. Jansen, H. Hölscher, H. Fuchs, and A. Schirmeisen, Phys. Rev. Lett. **104**, 256101 (2010).
[31] A. Schirmeisen, L. Jansen, H. Hölscher, and H. Fuchs, Appl. Phys. Lett. **88**, 123108 (2006).
[32] X. Zhao, M. Hamilton, W. G. Sawyer, and S. S. Perry, Tribol. Lett. **27**, 113 (2007).
[33] X. Zhao, S. R. Phillpot, W. G. Sawyer, S. B. Sinnott, and S. S. Perry, Phys. Rev. Lett. **102**, 186102 (2009).
[34] N. Prodanov and A. Khomenko, Surf. Sci. **604**, 730 (2010).
[35] E. Gnecco, R. Bennewitz, T. Gyalog, C. Loppacher, M. Bammerlin, E. Meyer, and H. J. Güntherodt, Phys. Rev. Lett. **84**, 1172 (2000).